Volume 3
Number 19
7 October 2022
Pages 7145–7372

# Materials Advances

rsc.li/materials-advances

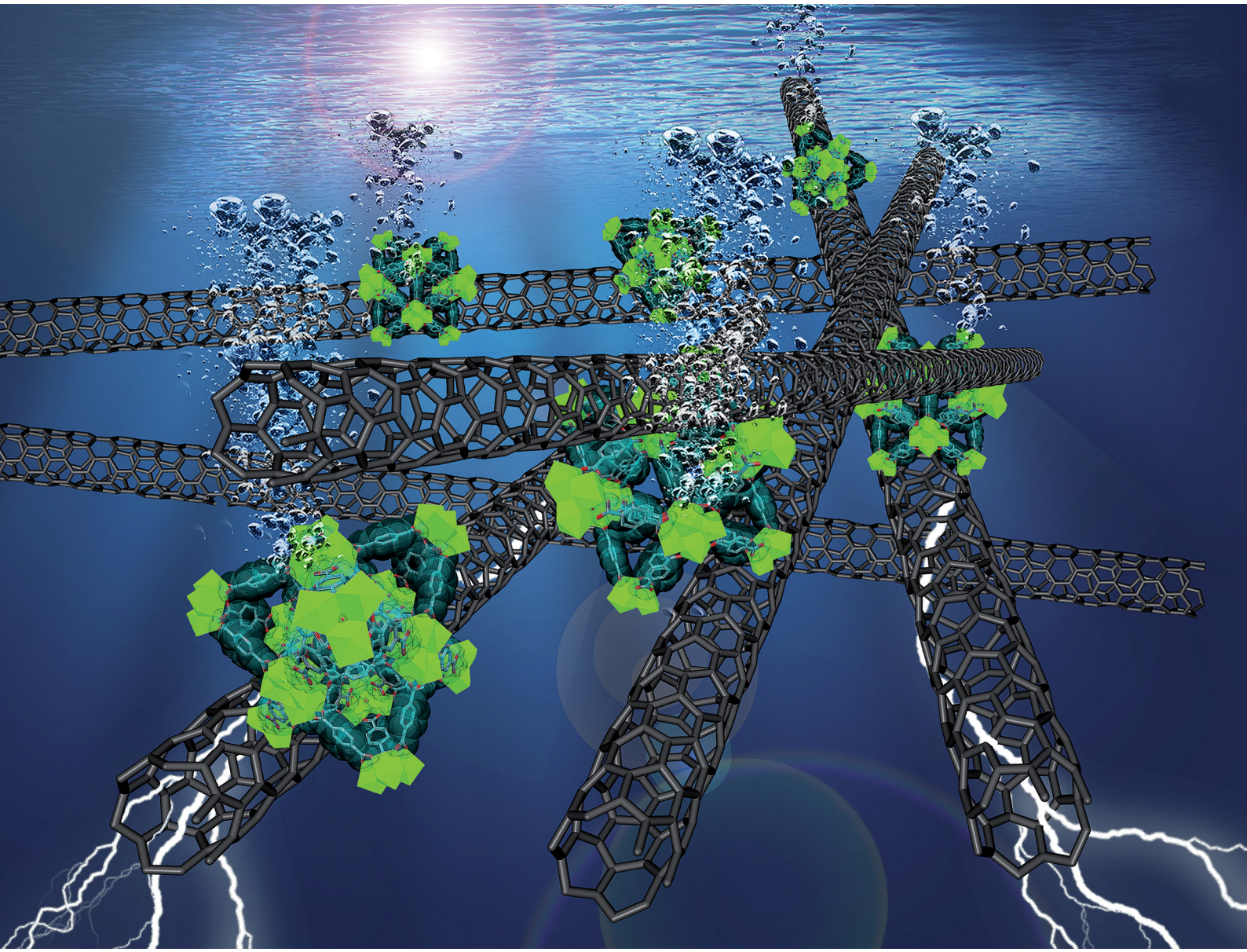

ISSN 2633-5409

ROYAL SOCIETY OF CHEMISTRY

**PAPER**

Mohamed H. Alkordi *et al.*

Synergistic compounding of carbon nanotubes and metal–organic frameworks for oxygen-evolving electrocatalysis

Materials Advances

ROYAL SOCIETY OF CHEMISTRY

PAPER

View Article Online
View Journal | View Issue



Cite this: *Mater. Adv.*, 2022, 3, 7212

# Synergistic compounding of carbon nanotubes and metal–organic frameworks for oxygen-evolving electrocatalysis

Mohamed H. Hassan, [ab] Rana R. Haikal [a] and Mohamed H. Alkordi *[a]

Received 29th March 2022,
Accepted 20th July 2022

DOI: 10.1039/d2ma00361a

rsc.li/materials-advances

In this report, we demonstrate that utilizing multi-walled carbon nanotubes (MWCNTs) coated with a microporous metal–organic framework (UiO-66-$NH_2$) that was doped with electrocatalytically active Ni(II) ions can produce a highly efficient heterogeneous electrocatalyst for the water oxidation reaction. The electrode material demonstrated an onset potential for the OER of 1.51 V *vs.* RHE (overpotential $\eta$ = 0.28 V) and an outstanding overpotential at a current density of 10 mA $cm^{-2}$ ($\eta_{10}$ = 0.33 V), ultimately reaching a considerably high current density of 600 mA $cm^{-2}$ at 2.05 V *vs.* RHE. The prepared electrocatalyst demonstrated maintained catalytic activity in a highly caustic 1 M KOH solution for at least 7 hours of continuous controlled current electrolysis. This approach is synthetically appealing due to its applicability to several other systems through combining functional microporous MOF deposition on a conductive carbon support with minimal modifications, opening the door for cheap and efficient heterogeneous electrocatalysts for energy storage and conversion technologies.



## Introduction

Tapping the abundant, but otherwise intermittent, solar energy in a non-polluting manner has triggered active research into energy conversion technologies, in order to store and subsequently utilize the surplus of electrical energy produced through photovoltaic cells.[1–3] The water splitting process, through which solar-generated electrical energy could be stored in $H_2$ and $O_2$ is a viable option to consider.[4] The water oxidation reaction, known also as the oxygen evolution reaction (OER), is the most thermodynamically demanding reaction in water splitting, and thus catalysts that can facilitate this reaction at moderate energy expenses, and preferably demonstrate high efficiency in terms of catalyst cost and durability, are actively being pursued.[4] Although molecular catalysts, carefully designed after a specific reaction, can demonstrate high activity, their utilization in real world working conditions necessitates efficient immobilization within solid matrices.[5] In this regard, microporous solids, including metal–organic frameworks (MOFs), continue to demonstrate great potential in the area of heterogeneous catalysis.[6–8] MOFs possess several attractive attributes as solid matrices for establishing heterogeneous catalysis, including demonstrated reticular synthesis to fine-tune their structure.[9,10] The crystalline nature of MOFs facilitates studying their structure–function relationships,[11] which can further guide the design of specific MOFs for targeted applications. Moreover, MOFs are, in general, amenable for facile post-synthesis treatment processes, through which a certain MOF's activity can be further enhanced or even tailored.[12] Essential attributes of a porous solid support for utilization in heterogeneous catalysis include demonstrated chemical and thermal stability, as well as enhanced support-catalyst interactions necessary to prevent catalyst leaching and thus ensure durability.[13] Although MOFs have recently been successfully employed in a myriad of thermally-promoted catalytic reactions,[14] them being electrical insulators has precluded their utilization in electrochemical heterogeneous catalysis.[15,16] Departing from O- or N-based organic linkers to S-based ones in the construction of MOFs appeared to provide a pathway to enhance the electrical conductivity in certain MOFs.[17] Alternatively, MOFs constructed from redox-active building blocks or containing certain guest molecules have also demonstrated enhanced electrical properties.[18,19] Previously, we demonstrated that Ni(II) ions immobilized on an amine-functionalized Zr-carboxylate MOF/graphene composite (UiO-66-$NH_2$@G) can be used as a precursor for generating a highly active $Ni(OH)_2$–$Zr(OH)_4$ catalyst on graphene for the OER.[20] This catalyst is formed *in situ* during MOF degradation in a highly alkaline environment leading to the formation of dispersed metal hydroxide nanoparticles on graphene sheets.

[a] *Center for Materials Science, Zewail City of Science and Technology, 5th of October, Giza 12578, Egypt. E-mail: malkordi@zewailcity.edu.eg, malkordi@mail.usf.edu*
[b] *Department of Chemistry and Biomolecular Science, Clarkson University, Potsdam, New York 13699, USA*

Herein, we describe a much more active electrocatalyst as compared to UiO-66-$NH_2$-Ni@G employing a 1D conductive support (multi-walled carbon nanotubes (MWCNTs)) with an exceedingly higher aspect ratio as compared to G.[21,22]

## Experimental

All reagents were used as received without further purification, purchased from Sigma-Aldrich or Fisher Scientific-UK. Nitrogen gas for sorption was purchased from Airliquide ($N_2$ AlphaGaz2 (99.999%). Carbon nanotubes (Alfa Aesar Fullerene, nanotube, multi-walled, 20 nm OD, 5–20 micron long 50 mg, Stock #: 43839, Lot # J30L17) were used as received without further purification. Solution pH was measured using a HANNA instruments HI-5522 pH meter calibrated as per the recommendations of the manufacturer.

### Gas sorption analysis

Gas sorption analysis was performed on a Micromeretics ASAP2020. The apparent surface areas were determined from the nitrogen adsorption isotherms collected at 77 K by applying the Brunauer–Emmett–Teller (BET) and Langmuir models. Pore size analyses were performed using an NLDFT for the cylinder pore model system, assuming an oxide surface.

Infrared absorption spectra were recorded on a Thermo-Scientific Nicolet is-10. Thermogravimetric analyses were conducted on a Thermal Analysis-Q50. SEM images were acquired on a NOVA NanoSEM 450, operating at 30 kV.

### Electrochemical measurements

In a typical run, 1.22 mg of the UiO-66-$NH_2$-Ni@MWCNTs was dispersed in 0.5 mL of isopropanol and sonicated briefly to prepare the ink, of which 40 μL was drop cast on a freshly polished GCE of 3 mm diameter. The electrochemical measurements were conducted on a biologic SP-50 potentiostat/galvanostat in a three electrode configuration. The working electrode was a GCE cast with the prepared ink, Pt wire as a counter electrode and a saturated sodium chloride calomel electrode (SSCE) as a reference electrode; the measured potential values were then converted to RHE using a standard potential of 0.236 V for the SSCE *vs.* NHE. The electrolyte was aqueous KOH (1 M, pH = 13.8). Electrocatalytic response was measured using the linear sweep voltammetry (LSV) technique, the cyclic voltammetry technique (CV), or the controlled current chronopotentiometry technique (CP). The working electrode potential was swept at a scan rate of 10 mV $s^{-1}$ for the LSV, while the cyclic voltammetry was measured with a scan rate of 100 mV $s^{-1}$ or 50 mV $s^{-1}$ as indicated.

### Synthesis of UiO-66-$NH_2$@MWCNTs and Ni metallation

Into two separate vials, solution A was made by dissolving 2-aminoterephthalic acid (45 mg, 0.248 mmol) and suspending 50 mg of MWCNTs in 10 mL DMF. Solution B was made by dissolving $ZrCl_4$ (42 mg, 0.18 mmol) in 5 ml DMF and 1 mL HCl (37 wt%). Both solutions were sonicated for 20 min and then the $ZrCl_4$ solution was dropped into solution A while stirring; the vial was sealed and kept stirring at 400 rpm with a stirring bar in a sand bath at 80 °C for 18 h. The contents were then filtered when cooled and washed many times with acetonitrile and soaked in ACN for 2 h in a sealed vial at 80 °C under autogenous pressure. The solid was then filtered and dried in an oven for 1 h at 80 °C to produce a black solid (100 mg). For Ni loading, 40 mg of the product was incubated in 0.1 M $Ni(NO_3)_2{\cdot}6H_2O$ in 15 mL ACN for 1 h at 80 °C in a sealed vial under autogenous pressure, cooled, then filtered and washed with ACN and soaked in ACN for 1 h at room temp, then filtered, washed again with ACN and dried at 80 °C.

## Results and discussion

The high aspect ratio of the MWCNTs and G provided good electrical conductivity within the composites containing MWCNTs or G fillers, with favorably low filler wt% due to an early onset of the conductivity percolation threshold.[23] The strategy adopted here is to utilize solvothermal synthesis of UiO-66-$NH_2$ in the presence of dispersed MWCNTs resulting in homogenous nucleation and thus coverage of the MWCNTs with MOF nanoparticles, aided by mechanical stirring of the reaction mixture. The MWCNTs were selected as a support upon which the MOF was constructed in order to overcome the poor electrical conductivity of the MOF, acting as a nanowire mesh imbedded within the composite. The subsequent impregnation with Ni(II) ions was straightforwardly attained through the wetness impregnation method, in a solution of $Ni(NO_3)_2$ salt in acetonitrile. Ni(II) ion metallation was attempted to load the microporous matrix with cheap, abundant, and yet catalytically active metal ions towards the electrocatalytic OER.[24]

The composite can then be regarded as MWCNTs sensitized/functionalized by the active microporous, Ni-doped MOF. An essential aspect of this design is the retained electrocatalytic activity of the composite even after the MOF's degradation in a basic solution. Indeed, the effective compounding of the two materials was evidenced through Fourier-transform infrared spectroscopy (FTIR, Fig. 1), which demonstrated close similarity between the spectra of UiO-66-$NH_2$ and the UiO-66-$NH_2$-Ni@MWCNTs composite. The FTIR spectra of UiO-66-$NH_2$ and its composite demonstrated the characteristic peaks at around 1553 and 1378 $cm^{-1}$ related to the asymmetric and symmetric vibrations of the Zr-bonded carboxylate groups, respectively. The disappearance of the peak at 1649 $cm^{-1}$ after Ni immobilization might be ascribed to N–H bending vibration that is affected with Ni coordination or the removal of trace DMF left within the MOF pores.

The scanning electron microscopy (SEM) images for the UiO-66-$NH_2$-Ni@MWCNTs are shown in Fig. 2. As displayed in the lower magnification image, solid particles of apparently homogenous composition are visible. Upon magnification, a network of MWCNTs imbedded within a large number of MOF nanoparticles became apparent, evidencing the tight entanglement of the MOF and the MWCNTs.

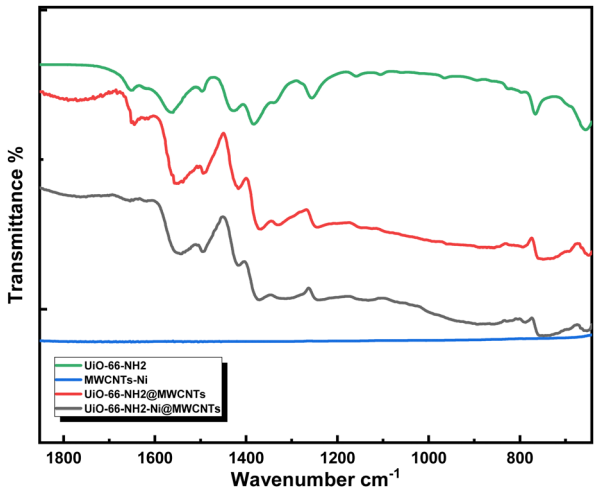


Fig. 1 FTIR spectra of the UiO-66-$NH_2$, UiO-66-$NH_2$@MWCNTs, and UiO-66-$NH_2$-Ni@MWCNTs in comparison with Ni-soaked MWCNTs.

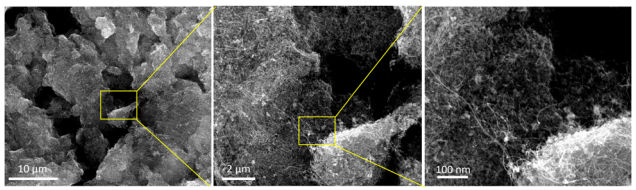


Fig. 2 SEM images at different magnifications of the UiO-66-$NH_2$-Ni@MWCNTs.

The energy-dispersive X-ray photoelectron spectroscopy (EDX), Fig. 3, of the Ni-loaded composite demonstrated the homogeneous distribution of Ni within the composite, where the Ni map essentially traced the elemental maps of the C, O, and Zr in the sample. Furthermore, the EDX analysis indicated a Ni loading of 1.8 wt% within the composite.

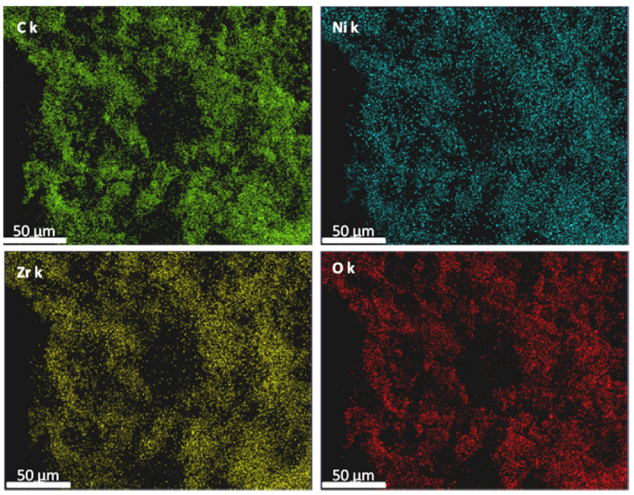


Fig. 3 EDX maps for UiO-66-$NH_2$-Ni@MWCNTs showing the homogenous distribution of the elements (labeled images) throughout the sample.

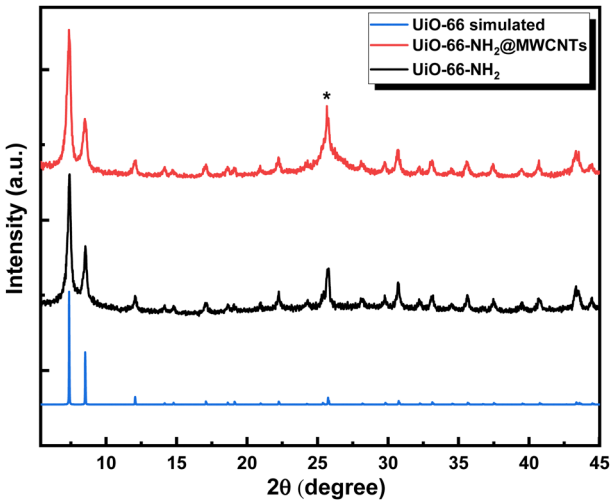


Fig. 4 XRD diffraction patterns for the UiO-66-$NH_2$@ MWCNTs, UiO-66-$NH_2$ and simulated UiO-66. The asterisk indicates the (002) diffraction peak related to MWCNTs.

The successful construction of the MOF within MWCNTs was further supported through X-ray powder diffraction (XRD), Fig. 4. The XRD pattern recorded for the MOF@MWCNTs matched that of the pristine MOF, with an additional broad peak at $2\theta$ = 25.7° characteristic of the MWCNTs.[25] No additional peaks were observed that can be ascribed to other crystalline $Ni(OH)_2$ phases, further supporting the assumption of atomistic/ionic Ni(II) species anchored within the MOF, *vide infra*. The thermal stability of the composite was assessed using thermogravimetric analysis (TGA, Fig. 5) and demonstrated comparable thermal stability to UiO-66-$NH_2$ up to *ca.* 400 °C.[21]

A noticeable weight loss step commenced at 300 °C for the composite metallated with Ni(II) and could potentially be ascribed to Ni-catalyzed thermal decomposition of the amine functional groups, and/or decomposition of the nitrate counter ions.

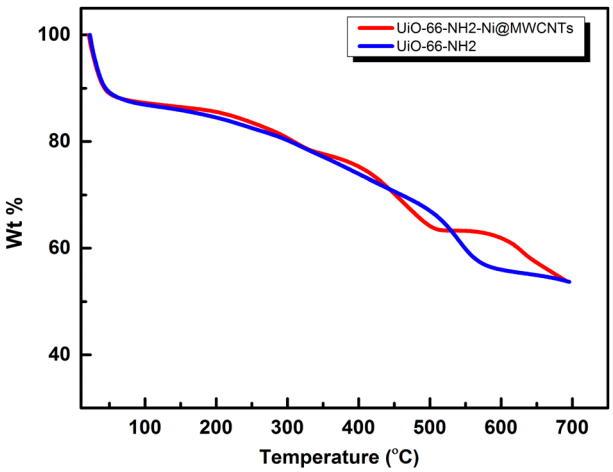


Fig. 5 TGA analysis for the UiO-66-$NH_2$ and the UiO-66-$NH_2$-Ni@MWCNTs.

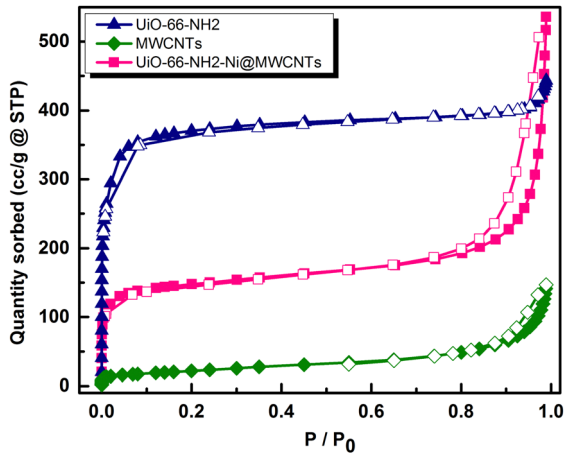


Fig. 6 $N_2$ sorption isotherms for UiO-66-$NH_2$, MWCNTs and UiO-66-$NH_2$-Ni@MWCNTs.

To assess the microporosity of the composite, $N_2$ sorption isotherms were measured, Fig. 6, for the UiO-66-$NH_2$ and the Ni-loaded composite. The two compounds demonstrated type-I like isotherms indicating microporosity with calculated Brunauer–Emmett–Teller (BET) surface area (SA) values of 1256 $m^2\ g^{-1}$ and 504 $m^2\ g^{-1}$, respectively. The MWCNTs when tested demonstrated a SA of 78.7 $m^2\ g^{-1}$, indicating a major contribution of the MOF to the observed microporosity of the composite. The pore size distribution (PSD, Fig. 7) histograms indicated close similarity between the composite and the pristine MOF. Considering the mass of MWCNTs utilized in the synthesis of the UiO-66-$NH_2$@MWCNTs, and the isolated yield of the composite, a MOF contribution of 50 wt% to the composite was calculated. As the MWCNTs used in this study demonstrated a SA of 78.7 $m^2\ g^{-1}$, a weighted average SA of 667 $m^2\ g^{-1}$ was expected for the composite. The observed SA of 504 $m^2\ g^{-1}$ is thus well within the expected range, taking into consideration the expected further reduction in SA due to $Ni(NO_3)_2$ loading within the composite. It

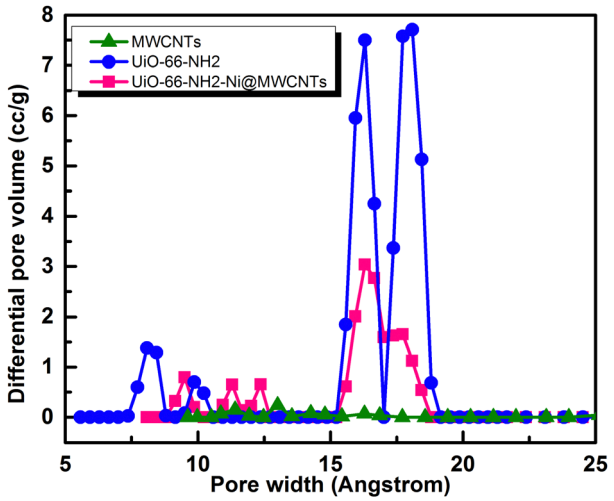


Fig. 7 Pore size distribution (PSD) histograms for the UiO-66-$NH_2$, MWCNTs, and UiO-66-$NH_2$-Ni@MWCNTs.

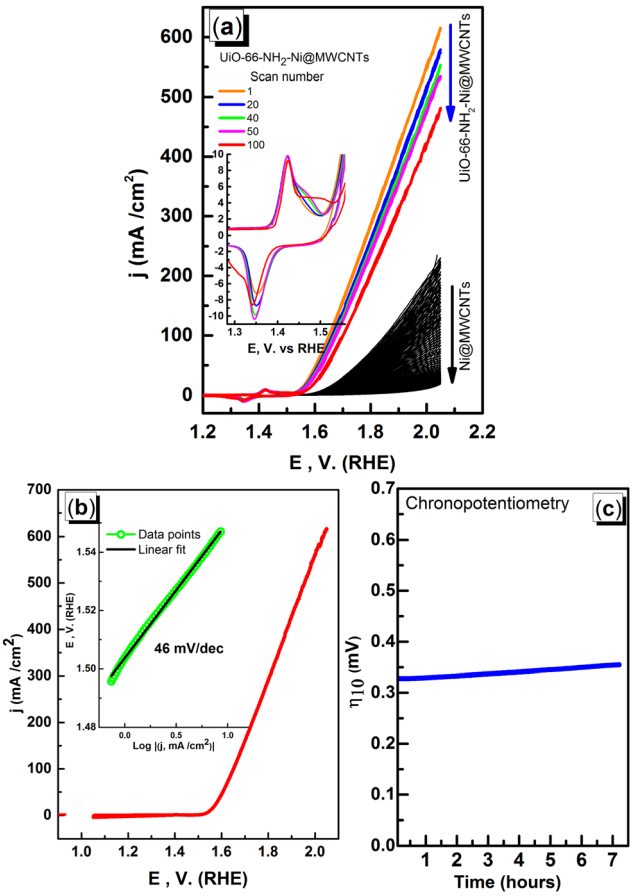


Fig. 8 (a) CV measurements for UiO-66-$NH_2$-Ni@MWCNTs (colored traces) with the inset showing the Ni(II/III) redox couple, and the Ni@MWCNTs control (black trace), (b) LSV scan showing the OER activity of the composite with the Tafel plot and linear fit in the inset, and (c) controlled current electrolysis for 7 h. Measurements were conducted in aerated 1 M KOH solution, with a scan rate of 100 mV $s^{-1}$ for the CVs and 10 mV $s^{-1}$ for the LSV.

has been well reported that the UiO-66 MOF family decompose under highly basic conditions.[26] This could be regarded as a drawback limiting their use in applications that necessitate such harsh working conditions. However, this aspect can be well-utilized to generate usable catalysts from the MOF degradation products. When the UiO-66-$NH_2$-Ni@MWCNTs electrode is soaked in electrolyte solution at pH $\sim$ 14, it is expected that the MOF will rapidly degrade. Due to the presence of Ni(II) in the MOF, most likely anchored at the amine groups or at the hydroxyl ions of the $Zr_6$ clusters, a mixed metal hydroxide is expected to be formed under this highly caustic environment to deposit Ni and/or Ni-Zr hydroxide coated on the MWCNTs, as previously observed on graphene platelets.[20] The cyclic voltammograms (CVs) of the Ni-loaded composite in 1 M KOH solution demonstrated a remarkable catalytic activity towards the OER, Fig. 8a. As a control, MWCNTs were soaked in $Ni(NO_3)_2$ solution under similar conditions utilized for doping the composite, and demonstrated little activity towards the OER, which rapidly decays due to Ni ion leaching. This poor performance is expected for weakly bound Ni ions on the surface of the MWCNTs. The 100 CV scans recorded

Table 1 Comparison of OER activity for some Ni-based catalysts

| Catalyst | $E_{onset}$ (V) *vs.* RHE | $\eta_{10}$ (V) | Tafel Slope (mV dec$^{-1}$) | Electrolyte | Ref. |
|---|---|---|---|---|---|
| UiO-66-$NH_2$-Ni@MWCNTs | 1.51 | **0.33** | **46** | 1 M KOH | This work |
| Ni@NiO/N-C nanowires | — | 0.39 | 100 | 1 M KOH | 28 |
| $NiCo_2O_4$/graphene | 1.50 | 0.383 | 137 | 1 M KOH | 29 |
| Zn-doped $NiCo_2O_4$ | 1.65 | 0.56 | 62 | 0.1 M KOH | 30 |
| $NiO_x$ | 1.59 | 0.427 | 117 | 0.1 M KOH | 31 |
| $IrO_x$ | 1.48 | 0.32 | 42 | 1 M NaOH | 4 |

on the composite demonstrated a nearly stable performance, and showed the characteristic Ni(II/III) redox pair indicative of the formation of the Ni(OOH) species at 1.4 V *vs.* RHE.[27] The linear sweep voltammogram (LSV), Fig. 8b, demonstrated the early onset potential for the OER (1.51 V *vs.* RHE, $\eta$ = 280 mV) and a considerably low overpotential at 10 mA cm$^{-2}$ current density ($\eta_{10}$ = 330 mV), ultimately reaching a considerably high current density of 600 mA cm$^{-2}$ at 2.05 V *vs.* RHE. Such observed electrocatalytic current and overpotentials are among the best reported values for OER catalysts,[4] even exceeding the range of 0.4 V overpotential predicted to be the thermodynamic overpotential for the OER at metal-oxide flat surfaces,[32] indicating the high activity of the composite. The Tafel slope for the OER, inset in Fig. 8b, was found to be 46 mV dec$^{-1}$, among the lowest reported for Ni-based catalysts for the OER, Table 1.[33,34] Such value of the Tafel slope can be taken to indicate facilitated kinetics of the OER within the composite,[27,35] which can tentatively be ascribed to efficient anchorage of the catalytic Ni(II) centers within the MOF degradation products and MWCNTs, acting primarily as the electron collector element.

It is reasonable to assume a crucial role of the MOF, as a highly porous sacrificial scaffold supplying anchoring sites for Ni(II) ions on the pendant amine functionality. After MOF degradation, the generated $Zr(OH)_4$ coprecipitated with $Ni(OH)_2$ plays an important role in the enhanced catalytic activity through the interplay between both components and MWCNTs. The catalytic performance of the composite under working conditions was probed through controlled current electrolysis, Fig. 8c. The maintained overpotential to support a working current density of 10 mA cm$^{-2}$ for a period of 7 hours clearly demonstrated the durability of the composite in the highly alkaline solution.

## Conclusion

Herein, we describe a one-pot synthesis and post synthetic metallation with Ni(II) ions to construct a catalytically active composite through solvothermal synthesis of UiO-66-$NH_2$ in the presence of suspended MWCNTs, aided by mechanical stirring. The Ni-loaded composite demonstrated high catalytic activity and durability towards the OER, as compared to a control experiment of Ni-treated MWCNTs, signifying the role of the MOF in providing a highly microporous scaffold to immobilize the solvent-accessible Ni(II) species. As the UiO-66-$NH_2$-Ni did not show significant catalytic activity under similar conditions, the observed activity of the composite can be ascribed to the efficient compounding of its major three components. The reported approach can potentially be applied to several other MOFs, targeting platform materials for efficient energy conversion and storage applications with minimal modifications of the pristine MOF.

## Conflicts of interest

There are no conflicts to declare.

## Acknowledgements

We acknowledge the funds from Zewail City of Science and Technology, the Egyptian Science and Technology Development Fund (STDF, USC17-43), and the Alexander von Humboldt Foundation.

## References

1 S. Y. Reece, J. A. Hamel, K. Sung, T. D. Jarvi, A. J. Esswein, J. J. H. Pijpers and D. G. Nocera, Wireless Solar Water Splitting Using Silicon-Based Semiconductors and Earth-Abundant Catalysts, *Science*, 2011, **334**(6056), 645–648.
2 H. B. Gray, Powering the planet with solar fuel, *Nat. Chem.*, 2009, **1**(1), 7.
3 N. S. Lewis and D. G. Nocera, Powering the planet: Chemical challenges in solar energy utilization, *Proc. Natl. Acad. Sci. U. S. A.*, 2006, **103**(43), 15729–15735.
4 C. C. L. McCrory, S. Jung, J. C. Peters and T. F. Jaramillo, Benchmarking Heterogeneous Electrocatalysts for the Oxygen Evolution Reaction, *J. Am. Chem. Soc.*, 2013, **135**(45), 16977–16987.
5 R. R. Haikal, X. Wang, Y. S. Hassan, M. R. Parida, B. Murali, O. F. Mohammed, P. J. Pellechia, M. Fontecave and M. H. Alkordi, Porous–Hybrid Polymers as Platforms for Heterogeneous Photochemical Catalysis, *ACS Appl. Mater. Interfaces*, 2016, **8**(31), 19994–20002.
6 P. Kaur, J. T. Hupp and S. T. Nguyen, Porous Organic Polymers in Catalysis: Opportunities and Challenges, *ACS Catal.*, 2011, **1**(7), 819–835.
7 M. H. Alkordi, J. Weseliński, V. D'Elia, S. Barman, A. Cadiau, M. N. Hedhili, A. J. Cairns, R. G. AbdulHalim, J.-M. Basset and M. Eddaoudi, CO 2 conversion: the potential of porous-organic polymers (POPs) for catalytic CO 2–epoxide insertion, *J. Mater. Chem. A*, 2016, **4**(19), 7453–7460.

8 A. B. Soliman, R. R. Haikal, Y. S. Hassan and M. H. Alkordi, The potential of a graphene-supported porous-organic polymer (POP) for CO 2 electrocatalytic reduction, *Chem. Commun.*, 2016, **52**, 12032–12035.
9 O. M. Yaghi, M. O'keeffe, N. W. Ockwig, H. K. Chae, M. Eddaoudi and J. Kim, Reticular synthesis and the design of new materials, *Nature*, 2003, **423**(6941), 705–714.
10 R. G. AbdulHalim, A. Shkurenko, M. H. Alkordi and M. Eddaoudi, Supramolecular Isomers of Metal–Organic Frameworks Derived from a Partially Flexible Ligand with Distinct Binding Motifs, *Cryst. Growth Des.*, 2016, **16**(2), 722–727.
11 M. H. Alkordi, Y. Belmabkhout, A. Cairns and M. Eddaoudi, Metal–organic frameworks for H2 and CH4 storage: insights on the pore geometry–sorption energetics relationship, *IUCrJ*, 2017, **4**(2), 131–135.
12 S. J. Garibay, Z. Wang, K. K. Tanabe and S. M. Cohen, Postsynthetic Modification: A Versatile Approach Toward Multifunctional Metal-Organic Frameworks, *Inorg. Chem.*, 2009, **48**(15), 7341–7349.
13 M. H. Alkordi, Y. Liu, R. W. Larsen, J. F. Eubank and M. Eddaoudi, Zeolite-like metal– organic frameworks as platforms for applications: on metalloporphyrin-based catalysts, *J. Am. Chem. Soc.*, 2008, **130**(38), 12639–12641.
14 D. Farrusseng, S. Aguado and C. Pinel, Metal–Organic Frameworks: Opportunities for Catalysis, *Angew. Chem., Int. Ed.*, 2009, **48**(41), 7502–7513.
15 I. Hod, M. D. Sampson, P. Deria, C. P. Kubiak, O. K. Farha and J. T. Hupp, Fe-Porphyrin-Based Metal–Organic Framework Films as High-Surface Concentration, Heterogeneous Catalysts for Electrochemical Reduction of $CO_2$, *ACS Catal.*, 2015, **5**(11), 6302–6309.
16 E. M. Miner, T. Fukushima, D. Sheberla, L. Sun, Y. Surendranath and M. Dincă, Electrochemical oxygen reduction catalysed by Ni3(hexaiminotriphenylene)2, *Nat. Commun.*, 2016, **7**, 10942.
17 L. Sun, T. Miyakai, S. Seki and M. Dincă, Mn2(2,5-disulfhydrylbenzene-1,4-dicarboxylate): A Microporous Metal–Organic Framework with Infinite $(-Mn-S-)\infty$ Chains and High Intrinsic Charge Mobility, *J. Am. Chem. Soc.*, 2013, **135**(22), 8185–8188.
18 Y. Kobayashi, B. Jacobs, M. D. Allendorf and J. R. Long, Conductivity, Doping, and Redox Chemistry of a Microporous Dithiolene-Based Metal−Organic Framework, *Chem. Mater.*, 2010, **22**(14), 4120–4122.
19 S. Takaishi, M. Hosoda, T. Kajiwara, H. Miyasaka, M. Yamashita, Y. Nakanishi, Y. Kitagawa, K. Yamaguchi, A. Kobayashi and H. Kitagawa, Electroconductive Porous Coordination Polymer Cu[Cu(pdt)2] Composed of Donor and Acceptor Building Units, *Inorg. Chem.*, 2009, **48**(19), 9048–9050.
20 M. H. Hassan, A. B. Soliman, W. A. Elmehelmey, A. A. Abugable, S. G. Karakalos, M. Elbahri, A. Hassanien and M. H. Alkordi, A Ni-loaded, metal–organic framework–graphene composite as a precursor for in situ electrochemical deposition of a highly active and durable water oxidation nanocatalyst, *Chem. Commun.*, 2019, **55**(1), 31–34.
21 J. H. Cavka, S. Jakobsen, U. Olsbye, N. Guillou, C. Lamberti, S. Bordiga, K. P. Lillerud and A. New, Zirconium Inorganic Building Brick Forming Metal Organic Frameworks with Exceptional Stability, *J. Am. Chem. Soc.*, 2008, **130**(42), 13850–13851.
22 M. J. Katz, Z. J. Brown, Y. J. Colon, P. W. Siu, K. A. Scheidt, R. Q. Snurr, J. T. Hupp and O. K. Farha, A facile synthesis of UiO-66, UiO-67 and their derivatives, *Chem. Commun.*, 2013, **49**(82), 9449–9451.
23 M. E. A. Safy, R. R. Haikal, B. Elshazly, A. Hamdy, F. Ali, A. A. Maarouf and M. H. Alkordi, Charge percolation in metal-organic framework (HKUST-1)–graphene nanocomposites, *Appl. Mater. Today*, 2020, **19**, 100604.
24 M. S. Burke, L. J. Enman, A. S. Batchellor, S. Zou and S. W. Boettcher, Oxygen Evolution Reaction Electrocatalysis on Transition Metal Oxides and (Oxy)hydroxides: Activity Trends and Design Principles, *Chem. Mater.*, 2015, **27**(22), 7549–7558.
25 A. M. Baker, L. Wang, S. G. Advani and A. K. Prasad, Nafion membranes reinforced with magnetically controlled Fe3O4-MWCNTs for PEMFCs, *J. Mater. Chem.*, 2012, **22**(28), 14008–14012.
26 M. Ding, X. Cai and H.-L. Jiang, Improving MOF stability: approaches and applications, *Chem. Sci.*, 2019, **10**(44), 10209–10230.
27 L. Trotochaud, J. K. Ranney, K. N. Williams and S. W. Boettcher, Solution-Cast Metal Oxide Thin Film Electrocatalysts for Oxygen Evolution, *J. Am. Chem. Soc.*, 2012, **134**(41), 17253–17261.
28 A. Xie, J. Zhang, X. Tao, J. Zhang, B. Wei, W. Peng, Y. Tao and S. Luo, Nickel-based MOF derived Ni @ NiO/N–C nanowires with core-shell structure for oxygen evolution reaction, *Electrochim. Acta*, 2019, **324**, 134814.
29 Z. Li, B. Li, J. Chen, Q. Pang and P. Shen, Spinel NiCo2O4 3-D nanoflowers supported on graphene nanosheets as efficient electrocatalyst for oxygen evolution reaction, *Int. J. Hydrogen Energy*, 2019, **44**(31), 16120–16131.
30 M. Yang, Y. Li, Y. Yu, X. Liu, Z. Shi and Y. Xing, Self-Assembly of Three-Dimensional Zinc-Doped NiCo2O4 as Efficient Electrocatalysts for Oxygen Evolution Reaction, *Chem. – Eur. J.*, 2018, **24**(49), 13002–13008.
31 C. Zhu, D. Wen, S. Leubner, M. Oschatz, W. Liu, M. Holzschuh, F. Simon, S. Kaskel and A. Eychmüller, Nickel cobalt oxide hollow nanosponges as advanced electrocatalysts for the oxygen evolution reaction, *Chem. Commun.*, 2015, **51**(37), 7851–7854.
32 S. Jung, C. C. L. McCrory, I. M. Ferrer, J. C. Peters and T. F. Jaramillo, Benchmarking nanoparticulate metal oxide electrocatalysts for the alkaline water oxidation reaction, *J. Mater. Chem. A*, 2016, **4**(8), 3068–3076.
33 D. Mullangi, V. Dhavale, S. Shalini, S. Nandi, S. Collins, T. Woo, S. Kurungot and R. Vaidhyanathan, Low-Overpotential Electrocatalytic Water Splitting with Noble-

Metal-Free Nanoparticles Supported in a sp3N-Rich Flexible COF. *Advanced Energy*, *Materials*, 2016, **6**(13), 1600110.

34 S. Nandi, S. K. Singh, D. Mullangi, R. Illathvalappil, L. George, C. P. Vinod, S. Kurungot and R. Vaidhyanathan, Low Band Gap Benzimidazole COF Supported Ni3N as Highly Active OER Catalyst, *Adv. Energy Mater.*, 2016, 1601189.

35 J. C. B. Nadesan and A. C. C. Tseung, Oxygen Evolution on Nickel Oxide Electrodes, *J. Electrochem. Soc.*, 1985, **132**(12), 2957–2959.